

VI. COMPUTATIONAL VECTOR BME

The Bayesian Maximum Entropy (BME; Christakos, 1990, 1992) method may be extended to study two or more S/TRF that are related to each other. In this case the primary attribute is estimated by taking advantage of measurements from the other fields, referred to as the secondary fields, and the approach is called "vector BME". In this Chapter I present an extension of the formulations from the previous two Chapters for the case of vector BME involving the primary field and one secondary field. The method is then applied in a case study involving mortality and ambient temperature in the state of North Carolina.

6.1. What are Vector S/TRF's in BME Mapping?

The theory of Space/Time Random Fields presented in Chapter II may be extended under certain circumstances to study several S/TRF's related to each other (Christakos, 1992; Wackernagel, 1998). Letting $X(\mathbf{p})$ and $Y(\mathbf{p})$ be two related S/TRF's, we define their mean $m_x(\mathbf{p})$ and $m_y(\mathbf{p})$ as given by Eq. (2.6), and their covariance functions $c_x(\mathbf{p}, \mathbf{p}')$ and $c_y(\mathbf{p}, \mathbf{p}')$ as given by Eq. (2.7). We say that $X(\mathbf{p})$ and $Y(\mathbf{p})$ form a *vector* of S/TRF's, and we define an additional statistical moment of second order, namely the cross-covariance, as

$$\begin{aligned} c_{xy}(\mathbf{p}, \mathbf{p}') &= \overline{(X(\mathbf{p}) - m_x(\mathbf{p}))(Y(\mathbf{p}') - m_y(\mathbf{p}'))} \\ &= \iint (\chi - m_x(\mathbf{p}))(\psi - m_y(\mathbf{p}')) f_{xy}(\chi, \psi; \mathbf{p}, \mathbf{p}') d\chi d\psi \end{aligned} \quad (6.1)$$

where $f_{xy}(\chi, \psi; \mathbf{p}, \mathbf{p}')$ represents the bivariate pdf between the random fields X and Y taken at space-time points \mathbf{p} and \mathbf{p}' , respectively.

In the geostatistical framework, we define one of the S/TRF, say $X(\mathbf{p})$, as being the primary random field for which we are seeking an estimate χ_k at point \mathbf{p}_k , given general and specificatory information about both $X(\mathbf{p})$ and $Y(\mathbf{p})$. Following the usual notation we let $\boldsymbol{\chi}_{\text{hard}} = [\chi_1 \dots \chi_{m_h}]^T$ and $\boldsymbol{\chi}_{\text{soft}} = [\chi_{m_h+1} \dots \chi_m]^T$ represent the hard and soft data for the S/TRF $X(\mathbf{p})$ at m space/time points, $\boldsymbol{\psi}_{\text{hard}} = [\psi_1 \dots \psi_{n_h}]^T$ and $\boldsymbol{\psi}_{\text{soft}} = [\psi_{n_h+1} \dots \psi_n]^T$ represent the hard and soft data for the S/TRF $Y(\mathbf{p})$ at n space-time points, and $\boldsymbol{\chi}_{\text{data}}^T = [\boldsymbol{\chi}_{\text{hard}}^T \ \boldsymbol{\chi}_{\text{soft}}^T]$, $\boldsymbol{\psi}_{\text{data}}^T = [\boldsymbol{\psi}_{\text{hard}}^T \ \boldsymbol{\psi}_{\text{soft}}^T]$, and $\boldsymbol{\chi}_{\text{map}}^T = [\boldsymbol{\chi}_{\text{data}}^T \ \chi_k]$.

In BME mapping the Y_G -operator of Eq. (3.1) needs to be extended so as to account for joint general knowledge about $X(\mathbf{p})$ and $Y(\mathbf{p})$. The Y_G -operator will yield the prior pdf $f_G(\boldsymbol{\chi}_{\text{map}}, \boldsymbol{\psi}_{\text{data}})$, which is then used to define the Y_S -operator (see Eq. 3.3 and 3.4) that accounts for specificatory knowledge from both $X(\mathbf{p})$ and $Y(\mathbf{p})$. The operators for vector BME are presented next, and following I will give a proposed formulation for a case of practical interest, i.e. when the general knowledge includes mean, covariance and cross-covariance, which leads to an efficient numerical implementation.

6.2. The General Knowledge Operator

In the context of vector BME the general knowledge is expressed in terms of constraints of the form

$$\overline{g_\alpha} = \int d\boldsymbol{\chi}_{\text{map}} d\boldsymbol{\psi}_{\text{data}} f_G(\boldsymbol{\chi}_{\text{map}}, \boldsymbol{\psi}_{\text{data}}) g_\alpha(\boldsymbol{\chi}_{\text{map}}, \boldsymbol{\psi}_{\text{data}}) \quad (6.2)$$

where $\alpha = 0, 1, \dots, N_c$ and the $g_\alpha(\boldsymbol{\chi}_{\text{map}}, \boldsymbol{\psi}_{\text{data}})$ are given functions of χ_i 's and ψ_i 's. The the general knowledge operator Y_G accounts for this general knowledge by maximizing the entropy function

$$S[f_G] = - \int d\boldsymbol{\chi}_{\text{map}} d\boldsymbol{\Psi}_{\text{data}} f_G(\boldsymbol{\chi}_{\text{map}}, \boldsymbol{\Psi}_{\text{data}}) \log f_G(\boldsymbol{\chi}_{\text{map}}, \boldsymbol{\Psi}_{\text{data}}) \quad (6.3)$$

subject to the constraints (6.2). The solution to this constrained maximization problem is the prior pdf given by

$$f_G(\boldsymbol{\chi}_{\text{map}}, \boldsymbol{\Psi}_{\text{data}}) = Z^{-1} \exp[Y_G(\boldsymbol{\chi}_{\text{map}}, \boldsymbol{\Psi}_{\text{data}})] = Z^{-1} \exp\left[\sum_{\alpha=1}^{N_c} \mu_{\alpha} g_{\alpha}(\boldsymbol{\chi}_{\text{map}}, \boldsymbol{\Psi}_{\text{data}})\right] \quad (6.4)$$

where the N_c unknown coefficients μ_{α} are calculated from the N_c equations of Eqs. (6.2).

For convenience purposes we will use the following notation: We let \mathbf{x}_{hard} , \mathbf{x}_{soft} , x_k , \mathbf{y}_{hard} and \mathbf{y}_{soft} represent the vectors of random variables taking value $\boldsymbol{\chi}_{\text{hard}}$, $\boldsymbol{\chi}_{\text{soft}}$, $\boldsymbol{\chi}_k$, $\boldsymbol{\Psi}_{\text{hard}}$ and $\boldsymbol{\Psi}_{\text{soft}}$, respectively. Following the usual notation we write $\mathbf{x}_{\text{data}}^{\text{T}} = [\mathbf{x}_{\text{hard}}^{\text{T}} \mathbf{x}_{\text{soft}}^{\text{T}}]$, $\mathbf{x}_{\text{map}}^{\text{T}} = [\mathbf{x}_{\text{data}}^{\text{T}} x_k]$, $\mathbf{y}_{\text{data}}^{\text{T}} = [\mathbf{y}_{\text{hard}}^{\text{T}} \mathbf{y}_{\text{soft}}^{\text{T}}]$, and we define the \mathbf{z} vectors of random variable as follow: $\mathbf{z}_{\text{hard}}^{\text{T}} = [\mathbf{x}_{\text{hard}}^{\text{T}} \mathbf{y}_{\text{hard}}^{\text{T}}]$, $\mathbf{z}_{\text{soft}}^{\text{T}} = [\mathbf{x}_{\text{soft}}^{\text{T}} \mathbf{y}_{\text{soft}}^{\text{T}}]$, $\mathbf{z}_{\text{data}}^{\text{T}} = [\mathbf{x}_{\text{data}}^{\text{T}} \mathbf{y}_{\text{data}}^{\text{T}}]$ and $\mathbf{z}_{\text{map}}^{\text{T}} = [\mathbf{x}_{\text{map}}^{\text{T}} \mathbf{y}_{\text{data}}^{\text{T}}]$. Let's also define the covariance matrix $C_{\mathbf{x}, \mathbf{y}}$ for any two vectors $\mathbf{x} = [x_1 \dots x_m]^{\text{T}}$ and $\mathbf{y} = [y_1 \dots y_n]^{\text{T}}$ as

$$C_{\mathbf{x}, \mathbf{y}} = \overline{(\mathbf{x} - \bar{\mathbf{x}})(\mathbf{y} - \bar{\mathbf{y}})^{\text{T}}} = \begin{bmatrix} (x_1 - \bar{x}_1)(y_1 - \bar{y}_1) & \dots & (x_1 - \bar{x}_1)(y_n - \bar{y}_n) \\ \vdots & & \\ (x_m - \bar{x}_m)(y_1 - \bar{y}_1) & \dots & (x_m - \bar{x}_m)(y_n - \bar{y}_n) \end{bmatrix}. \quad (6.5)$$

One type of general knowledge that is of interest in spatiotemporal mapping is a general knowledge consisting of the mean's $m_x(\mathbf{p})$ and $m_y(\mathbf{p})$, the covariance functions $c_x(\mathbf{p}, \mathbf{p}')$ and $c_y(\mathbf{p}, \mathbf{p}')$ and the cross-covariance function $c_{xy}(\mathbf{p}, \mathbf{p}')$ for the S/TRF $X(\mathbf{p})$ and $Y(\mathbf{p})$, usually obtained by fitting to experimental data. In this case the prior pdf provided by the general knowledge operator is the multivariate Gaussian pdf given by

$$f_G(\boldsymbol{\chi}_{\text{map}}, \boldsymbol{\Psi}_{\text{data}}) = \phi([\boldsymbol{\chi}_{\text{map}}^T, \boldsymbol{\Psi}_{\text{data}}^T]^T; [\bar{\boldsymbol{x}}_{\text{map}}^T, \bar{\boldsymbol{y}}_{\text{data}}^T]^T, \boldsymbol{C}_{\text{map}}) \quad (6.6)$$

where $\phi(\boldsymbol{x}; \bar{\boldsymbol{x}}, \boldsymbol{C})$ denote the n -point Gaussian pdf of the random vector \boldsymbol{x} with mean $\bar{\boldsymbol{x}}$ and covariance matrix \boldsymbol{C} as defined in Eq. (4.4), and $\boldsymbol{C}_{\text{map}}$ is given by

$$\boldsymbol{C}_{\text{map}} = \boldsymbol{C}_{z_{\text{map}}, z_{\text{map}}} = \overline{(z_{\text{map}} - \bar{z}_{\text{map}})(z_{\text{map}} - \bar{z}_{\text{map}})^T}. \quad (6.7)$$

We note that the covariance matrix $\boldsymbol{C}_{\text{map}}$ may be partitioned as follow

$$\boldsymbol{C}_{\text{map}} = \begin{bmatrix} \boldsymbol{C}_{x_{\text{map}}, x_{\text{map}}} & \boldsymbol{C}_{x_{\text{map}}, y_{\text{data}}} \\ \boldsymbol{C}_{y_{\text{data}}, x_{\text{map}}} & \boldsymbol{C}_{y_{\text{data}}, y_{\text{data}}} \end{bmatrix} \quad (6.8)$$

where $\boldsymbol{C}_{x_{\text{map}}, x_{\text{map}}}$ is calculated using the covariance function $c_x(\boldsymbol{p}, \boldsymbol{p}')$, $\boldsymbol{C}_{y_{\text{data}}, y_{\text{data}}}$ is calculated using $c_y(\boldsymbol{p}, \boldsymbol{p}')$, and $\boldsymbol{C}_{y_{\text{data}}, x_{\text{map}}}$ is calculated using the cross-covariance function $c_{xy}(\boldsymbol{p}, \boldsymbol{p}')$.

6.3. The Specificatory Knowledge Operator

The processing operator Y_S which accounts for specificatory knowledge from both $X(\boldsymbol{p})$ and $Y(\boldsymbol{p})$ yields the BME posterior pdf as follow

$$f_K(\boldsymbol{\chi}_k) = A^{-1} Y_S[\boldsymbol{\chi}_{\text{soft}}, \boldsymbol{\Psi}_{\text{soft}}, Y_G(\boldsymbol{\chi}_{\text{map}}, \boldsymbol{\Psi}_{\text{data}})] \quad (6.9)$$

so that $f_G(\boldsymbol{\chi}_{\text{map}}, \boldsymbol{\Psi}_{\text{data}}) = Z^{-1} \exp[Y_G(\boldsymbol{\chi}_{\text{map}}, \boldsymbol{\Psi}_{\text{data}})]$ is the prior pdf.

When the specificatory knowledge consist of the hard data $\boldsymbol{\chi}_{\text{hard}}$ and $\boldsymbol{\psi}_{\text{hard}}$ and soft data of the interval type as given by Eq. (2.26), i.e. $P[l_x \leq \boldsymbol{x}_{\text{soft}} \leq \boldsymbol{u}_x] = 1$ and $P[l_y \leq \boldsymbol{y}_{\text{soft}} \leq \boldsymbol{u}_y] = 1$, then the Y_S -operator provides the following BME posterior pdf

$$f_K(\boldsymbol{\chi}_k) = A^{-1} \int_{l_x}^{u_x} d\boldsymbol{\chi}_{\text{soft}} \int_{l_y}^{u_y} d\boldsymbol{\psi}_{\text{soft}} f_G(\boldsymbol{\chi}_{\text{map}}, \boldsymbol{\psi}_{\text{data}}) \quad (6.10)$$

where A is the normalization constant defined in the usual way.

When the specificatory knowledge consist of the hard data $\boldsymbol{\chi}_{\text{hard}}$ and $\boldsymbol{\psi}_{\text{hard}}$ and soft data of the probabilistic type as given by Eq. (2.27), i.e. $P_S(\boldsymbol{x}_{\text{soft}} \leq \boldsymbol{\xi}_x, \boldsymbol{y}_{\text{soft}} \leq \boldsymbol{\xi}_y) = \int_{-\infty}^{\xi_x} d\boldsymbol{\chi}_{\text{soft}} \int_{-\infty}^{\xi_y} d\boldsymbol{\psi}_{\text{soft}} f_S(\boldsymbol{\chi}_{\text{soft}}, \boldsymbol{\psi}_{\text{soft}})$, then the Y_S -operator provides the following BME posterior pdf

$$f_K(\boldsymbol{\chi}_k) = A^{-1} \int d\boldsymbol{\chi}_{\text{soft}} \int d\boldsymbol{\psi}_{\text{soft}} f_S(\boldsymbol{\chi}_{\text{soft}}, \boldsymbol{\psi}_{\text{soft}}) f_G(\boldsymbol{\chi}_{\text{map}}, \boldsymbol{\psi}_{\text{data}}) \quad (6.11)$$

where A is the normalization constant defined in the usual way.

The BME method may be computationally intensive in general due to its flexibility, hence in order to produce a useful code I propose in the following a formulation which accounts for general knowledge consisting of the means, the covariance functions and cross-covariance function. These formulations are straightforward extensions of that presented in Chapter IV and V, and they will lead to an efficient numerical implementation.

6.4. A Proposed Formulation of the BME Posterior PDF for Efficient Computation

Let's assume that the general knowledge consisting of the means, the covariance functions and cross-covariance function of the S/TRF's $X(\mathbf{p})$ and $Y(\mathbf{p})$. Then the prior pdf is the multivariate Gaussian pdf given by Eq. (6.6). Using the notation of (6.5), let's define the following matrices: $\mathbf{C}_{h,h} = \mathbf{C}_{z_{\text{hard}},z_{\text{hard}}}$, $\mathbf{C}_{s,s} = \mathbf{C}_{z_{\text{soft}},z_{\text{soft}}}$, $\mathbf{C}_{k,k} = \mathbf{C}_{x_k,x_k}$, $\mathbf{C}_{h,s} = \mathbf{C}_{z_{\text{hard}},z_{\text{soft}}}$, $\mathbf{C}_{s,h} = \mathbf{C}_{h,s}^T$, $\mathbf{C}_{h,k} = \mathbf{C}_{z_{\text{hard}},x_k}$, $\mathbf{C}_{k,h} = \mathbf{C}_{h,k}^T$, $\mathbf{C}_{s,k} = \mathbf{C}_{z_{\text{soft}},x_k}$ and $\mathbf{C}_{k,s} = \mathbf{C}_{s,k}^T$. Let the aggregate matrices $\mathbf{C}_{kh,kh}$ and $\mathbf{C}_{hs,hs}$ be defined by

$$\mathbf{C}_{kh,kh} = \begin{bmatrix} \mathbf{C}_{k,k} & \mathbf{C}_{k,h} \\ \mathbf{C}_{h,k} & \mathbf{C}_{h,h} \end{bmatrix} \text{ and } \mathbf{C}_{hs,hs} = \begin{bmatrix} \mathbf{C}_{h,h} & \mathbf{C}_{h,s} \\ \mathbf{C}_{s,h} & \mathbf{C}_{s,s} \end{bmatrix}. \quad (6.12)$$

When the soft data is of the interval type, the BME posterior pdf of Eq. (6.10) may be written in the following convenient form for numerical computation

$$f_K(\chi_k) = A'^{-1} \phi(\chi_k; \mathbf{B}_{k|h} \boldsymbol{\zeta}_{\text{hard}}, \mathbf{C}_{k|h}) \int_{I_x}^{\mu_x} d\boldsymbol{\chi}_{\text{soft}} \int_{I_y}^{\mu_y} d\boldsymbol{\psi}_{\text{soft}} \phi(\boldsymbol{\chi}_{\text{soft}}, \boldsymbol{\psi}_{\text{soft}}; \mathbf{B}_{s|kh} \boldsymbol{\zeta}_{kh}, \mathbf{C}_{s|kh}) \quad (6.13)$$

where $\boldsymbol{\zeta}_{\text{hard}}^T = [\boldsymbol{\chi}_{\text{hard}}^T \boldsymbol{\psi}_{\text{hard}}^T]$, $\boldsymbol{\zeta}_{kh}^T = [\chi_k \boldsymbol{\zeta}_{\text{hard}}^T]$, $\mathbf{B}_{k|h} = \mathbf{C}_{k,h} \mathbf{C}_{h,h}^{-1}$, $\mathbf{C}_{k|h} = \mathbf{C}_{k,k} - \mathbf{B}_{k|h} \mathbf{C}_{h,k}$, $\mathbf{B}_{s|kh} = \mathbf{C}_{s,kh} \mathbf{C}_{kh,kh}^{-1}$, $\mathbf{C}_{s|kh} = \mathbf{C}_{s,s} - \mathbf{B}_{s|kh} \mathbf{C}_{kh,s}$, and $A' = \int_{I_x}^{\mu_x} d\boldsymbol{\chi}_{\text{soft}} \int_{I_y}^{\mu_y} d\boldsymbol{\psi}_{\text{soft}} \phi(\boldsymbol{\chi}_{\text{soft}}, \boldsymbol{\psi}_{\text{soft}}; \mathbf{B}_{s|kh} \boldsymbol{\zeta}_{\text{hard}}, \mathbf{C}_{s|kh})$.

When the soft data is of the probabilistic type, the BME posterior pdf of Eq. (6.11) takes the following form

$$f_K(\chi_k) = A'^{-1} \phi(\chi_k; \mathbf{B}_{k|h} \boldsymbol{\zeta}_{\text{hard}}, \mathbf{C}_{k|h}) \int d\boldsymbol{\chi}_{\text{soft}} d\boldsymbol{\psi}_{\text{soft}} f_S(\boldsymbol{\chi}_{\text{soft}}, \boldsymbol{\psi}_{\text{soft}}) \phi(\boldsymbol{\chi}_{\text{soft}}, \boldsymbol{\psi}_{\text{soft}}; \mathbf{B}_{s|kh} \boldsymbol{\zeta}_{kh}, \mathbf{C}_{s|kh}) \quad (6.14)$$

where $A' = \int d\boldsymbol{\chi}_{\text{soft}} d\boldsymbol{\psi}_{\text{soft}} f_S(\boldsymbol{\chi}_{\text{soft}}, \boldsymbol{\psi}_{\text{soft}}) \phi(\boldsymbol{\chi}_{\text{soft}}, \boldsymbol{\psi}_{\text{soft}}; \mathbf{B}_{s|h} \boldsymbol{\zeta}_{\text{hard}}, \mathbf{C}_{s|h})$.

6.5. Moments of the BME Posterior PDF

The mean $\bar{x}_{k|K} = \int \chi_k \chi_k f_K(\chi_k)$ of the BME posterior pdf, also called the conditional mean, is obtained for soft data of the interval type by using the BME posterior pdf of Eq. (6.13).

After some manipulations we get

$$\bar{x}_{k|K} = A'^{-1} \int_{I_x}^{u_x} d\boldsymbol{\chi}_{\text{soft}} \int_{I_y}^{u_y} d\boldsymbol{\psi}_{\text{soft}} \mathbf{B}_{k|hs} \boldsymbol{\zeta}_{\text{data}} \phi(\boldsymbol{\chi}_{\text{soft}}, \boldsymbol{\psi}_{\text{soft}}; \mathbf{B}_{s|h} \boldsymbol{\zeta}_{\text{hard}}, \mathbf{C}_{s|h}) \quad (6.15)$$

where $\mathbf{B}_{k|hs} = \mathbf{C}_{k,hs} \mathbf{C}_{hs,hs}^{-1}$, $\mathbf{C}_{k|hs} = \mathbf{C}_{k,k} - \mathbf{B}_{k|hs} \mathbf{C}_{hs,k}$, $\mathbf{B}_{s|h} = \mathbf{C}_{s,h} \mathbf{C}_{h,h}^{-1}$, $\mathbf{C}_{s|h} = \mathbf{C}_{s,s} - \mathbf{B}_{s|h} \mathbf{C}_{h,s}$ and $A' = \int_{I_x}^{u_x} d\boldsymbol{\chi}_{\text{soft}} \int_{I_y}^{u_y} d\boldsymbol{\psi}_{\text{soft}} \phi(\boldsymbol{\chi}_{\text{soft}}, \boldsymbol{\psi}_{\text{soft}}; \mathbf{B}_{s|h} \boldsymbol{\zeta}_{\text{hard}}, \mathbf{C}_{s|h})$.

In the case of soft data of the probabilistic type, using Eq. (6.14) leads to the following mean

$$\bar{x}_{k|K} = A'^{-1} \int d\boldsymbol{\chi}_{\text{soft}} d\boldsymbol{\psi}_{\text{soft}} f_S(\boldsymbol{\chi}_{\text{soft}}, \boldsymbol{\psi}_{\text{soft}}) \mathbf{B}_{k|hs} \boldsymbol{\zeta}_{\text{data}} \phi(\boldsymbol{\chi}_{\text{soft}}, \boldsymbol{\psi}_{\text{soft}}; \mathbf{B}_{s|h} \boldsymbol{\zeta}_{\text{hard}}, \mathbf{C}_{s|h}) \quad (6.16)$$

where $A' = \int d\boldsymbol{\chi}_{\text{soft}} d\boldsymbol{\psi}_{\text{soft}} f_S(\boldsymbol{\chi}_{\text{soft}}, \boldsymbol{\psi}_{\text{soft}}) \phi(\boldsymbol{\chi}_{\text{soft}}, \boldsymbol{\psi}_{\text{soft}}; \mathbf{B}_{s|h} \boldsymbol{\zeta}_{\text{hard}}, \mathbf{C}_{s|h})$.

Note that in the limiting case where only hard data is used, both Eq. (6.15) and (6.16) simplifies to the Simple Cokriging estimator:

$$\bar{x}_{k|K} = \mathbf{B}_{k|h} \boldsymbol{\zeta}_{\text{hard}} = [\mathbf{C}_{x_k, x_{\text{hard}}} \quad \mathbf{C}_{x_k, y_{\text{hard}}}] \begin{bmatrix} \mathbf{C}_{x_{\text{hard}}, x_{\text{hard}}} & \mathbf{C}_{x_{\text{hard}}, y_{\text{hard}}} \\ \mathbf{C}_{y_{\text{hard}}, x_{\text{hard}}} & \mathbf{C}_{y_{\text{hard}}, y_{\text{hard}}} \end{bmatrix}^{-1} \begin{bmatrix} \boldsymbol{\chi}_{\text{hard}} \\ \boldsymbol{\psi}_{\text{hard}} \end{bmatrix} \quad (6.17)$$

Similarly we may obtain the variance $\sigma_{k|K}^2 = \int d\chi_k (\chi_k - \bar{x}_{k|K})^2 f_K(\chi_k)$ of the BME posterior pdf. In the case of soft data of the interval type we get

$$\sigma_{k|K}^2 = C_{k|hs} + A'^{-1} \int_{I_x}^{u_x} d\boldsymbol{\chi}_{\text{soft}} \int_{I_y}^{u_y} d\boldsymbol{\psi}_{\text{soft}} (\mathbf{B}_{k|hs} \boldsymbol{\zeta}_{\text{data}} - \bar{x}_{k|K})^2 \phi(\boldsymbol{\chi}_{\text{soft}}, \boldsymbol{\psi}_{\text{soft}}; \mathbf{B}_{s|h} \boldsymbol{\zeta}_{\text{hard}}, \mathbf{C}_{s|h}) \quad (6.18)$$

where $A' = \int_{I_x}^{u_x} d\boldsymbol{\chi}_{\text{soft}} \int_{I_y}^{u_y} d\boldsymbol{\psi}_{\text{soft}} \phi(\boldsymbol{\chi}_{\text{soft}}, \boldsymbol{\psi}_{\text{soft}}; \mathbf{B}_{s|h} \boldsymbol{\zeta}_{\text{hard}}, \mathbf{C}_{s|h})$, while for soft data of the probabilistic type we have

$$\sigma_{k|K}^2 = C_{k|hs} + A'^{-1} \int d\boldsymbol{\chi}_{\text{soft}} d\boldsymbol{\psi}_{\text{soft}} f_S(\boldsymbol{\chi}_{\text{soft}}, \boldsymbol{\psi}_{\text{soft}}) (\mathbf{B}_{k|hs} \boldsymbol{\zeta}_{\text{data}} - \bar{x}_{k|K})^2 \phi(\boldsymbol{\chi}_{\text{soft}}, \boldsymbol{\psi}_{\text{soft}}; \mathbf{B}_{s|h} \boldsymbol{\zeta}_{\text{hard}}, \mathbf{C}_{s|h}) \quad (6.19)$$

with $A' = \int d\boldsymbol{\chi}_{\text{soft}} d\boldsymbol{\psi}_{\text{soft}} f_S(\boldsymbol{\chi}_{\text{soft}}, \boldsymbol{\psi}_{\text{soft}}) \phi(\boldsymbol{\chi}_{\text{soft}}, \boldsymbol{\psi}_{\text{soft}}; \mathbf{B}_{s|h} \boldsymbol{\zeta}_{\text{hard}}, \mathbf{C}_{s|h})$

6.6. Numerical implementation

By examining the equations for computational vector BME we find that there are a lot of similarities between the equation of this Chapter and those of Chapters IV and V. As a matter of fact the `BMEintEst` and `BMEpdfEst` programs can be extended to include one secondary S/TRF by redefining the covariance variables so that they include both covariance and cross-covariance effects, as illustrated in Eq. (6.8).

Using these principles I developed a vector version of the `BMEintEst` programs. By way of summary the input to the vector version of the `BMEintEst` programs includes the covariance function $c_x(\mathbf{p}, \mathbf{p}')$ for the primary S/TRF $X(\mathbf{p})$, the covariance function $c_y(\mathbf{p}, \mathbf{p}')$ for the secondary field $Y(\mathbf{p})$, the cross-covariance function $c_{xy}(\mathbf{p}, \mathbf{p}')$, the hard and soft interval data available for both $X(\mathbf{p})$ and $Y(\mathbf{p})$, and the space-time points where the estimation for $X(\mathbf{p})$ must be calculated. Note that the mean of the S/TRF's $X(\mathbf{p})$ and $Y(\mathbf{p})$ is assumed to be zero, which is equivalent to knowing the mean and subtracting it

from the hard and soft data. The output of the program consists in the (i) the mapping estimates (mode and mean of the posterior pdf), (ii) the variance of the posterior pdf (simple assessment of mapping accuracy), (iii) the BME confidence intervals (single-point error assessment).

It should be pointed out when calculating the mode of the BME posterior pdf, one can either use an equation of the type of Eq. (4.10), or simply use a numerical method to find the maximum of the posterior pdf. As it turns out the latter is always more efficient numerically, hence I did not need to give in this Chapter the extension of the Eq. (4.10) for vector BME.

The vector version of the BMEintEst programs were tested for correctness, and they were used in an epidemiology case study, as presented later.

6.7. Applications of Computational Vector BME in Environmental Sciences

Vector mapping describes an estimation approach using information from the primary attribute as well as related (secondary) attributes, whereas in *scalar* mapping only information from the primary attribute is used. Computational vector BME is a powerful method for vector mapping that accounts for hard and soft information from several related S/TRF's, and that obtains simple cokriging as a special case when only hard data is available. The obvious advantage of vector mapping over scalar mapping is that the added physical knowledge provided by the secondary S/TRF's results in a more accurate estimation of the primary attribute. This is of particular interest when the attributes are well correlated, and the primary attribute is under-sampled while a lot of measurements are available for the secondary attributes. Consider for example the case of the concentration of Cd and Ni in the soil (Goovaerts, 1997). These two attributes are correlated, hence,

when Cd is under-sampled, the vector estimation of Cd (using both attributes) is more informative than its scalar estimation (which uses only the under-sampled Cd data). By providing a rigorous framework accounting for hard and soft data, computational vector BME greatly expands the application of vector mapping to areas where uncertain physical knowledge about the related S/TRF's is available.

Another application of vector mapping in environmental health is the study of the causal association between an exposure field and its health effect on human population (Christakos and Serre, 1999). The analysis of disease/exposure associations is at the core of the epidemiology sciences, and vector spatiotemporal mapping provides a useful tool to investigate associations that present strong spatial and temporal characteristics. Consider for example the variations in space/time of a disease or a physiological condition in human population caused by some ambient air pollutant. Because of the strong space/time fluctuations of air pollutants, the association is best analyzed using a joint representation of disease rate and exposure by means of a vector formulation of S/TRF's. The exposure (cause) is considered the secondary attribute, while the disease rate (effect) is considered the primary attribute. The strength and accuracy of the disease/exposure causal association is evaluated by comparing the vector estimate of disease rate (using both primary and secondary attributes) with the scalar estimate of disease rate (which uses only information about the primary attribute). If the vector estimate is found to be more accurate than the scalar estimate, then the disease/exposure association exists. Furthermore the better the vector estimation compared to the scalar estimation, the stronger the disease/exposure association, thus offering a measure of the strength and consistency of the association in the space/time domain.

One of the challenge of analyzing disease/exposure associations is finding an adequate indicator of health effect in the human population, e.g. a measurable disease rate.

Often health indicators are measured indirectly, for example using counts of admissions in a hospital, or counts of death within a county. These counts are not continuous values of disease rate measured at a defined point in the space/time continuum, rather they include arbitrary factors such as the range covered by a hospital, or the boundary of a county. However these counts can be rigorously modelled as uncertain physical knowledge about an underlying S/TRF -- the disease rate. By accounting for uncertain physical knowledge, computational vector BME provides an accurate framework to analyze disease/exposure associations in the space/time domain. This is best shown using the case study about the analysis of the mortality/temperature association in North Carolina. Valuable insights are gained from this case study, which is presented next.

6.8. The Mortality/Temperature Association Case Study for North Carolina

The mortality/temperature association is an interesting example of association involving both spatial and temporal scales. In this case study (Christakos and Serre, 1999) we analyze the spatiotemporal association between temperature and mortality for the state of North Carolina for the 1995-1996 time period. The temperature-mortality relationship is known to have a V-shape, with both cold and hot temperature extremes resulting in higher death rates (Saez *et al.*, 1995; Honda *et al.*, 1995; Laake, 1996; Christophersen, 1997; Ballester-Diez, 1997; Choi *et al.*, 1997). However the study area did not experience any substantial hot temperature extreme for the time period considered (the daily mean temperature did not exceed 88 degrees Fahrenheit - less than the 91 degrees Fahrenheit threshold suggested by Honda *et al.*, 1995, for mortality increase induced by high temperature), and therefore only low temperature are considered as the environmental exposure leading to higher mortality. While previous studies focused generally on either the temporal (time series studies) or spatial (regional studies) aspects of the

mortality/temperature association, in this work we consider the combined spatiotemporal aspect of the association by means of the Space/Time Random Field (STRF) theory.

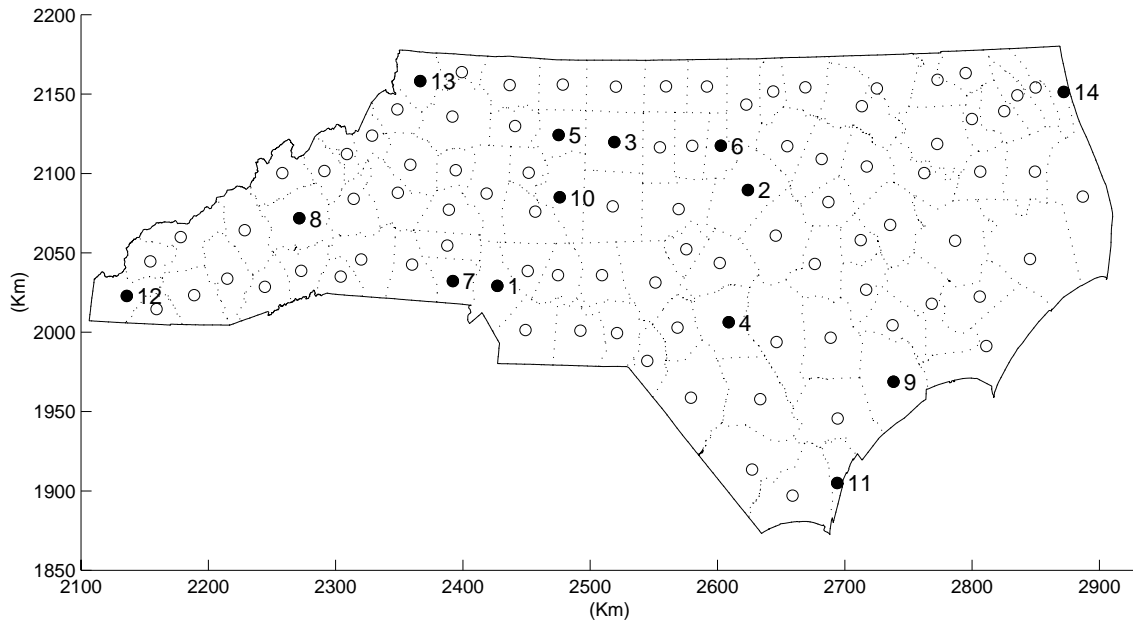


Figure 6.1: Map of North Carolina and its 100 counties. The centroids of each county are shown with circles. The 14 county selected for this study are numbered and have filled circles.

The state of North Carolina (Fig. 6.1) covers an area of approximately 800 Km by 300 Km, and is divided in one hundred counties. The boundaries of the counties are shown in dotted lines, and the location of the centroid of each county is depicted by a circle in Fig. 6.1. The ambient temperature for North Carolina is monitored by numerous weather stations located within the state. In Fig. 6.2 we show with triangles the location of eight weather stations for which daily mean temperatures were provided by the State Climate Office of North Carolina for the 1995-1996 time period. This network of weather stations provide an adequate coverage of the state, based upon which we created the map of annual mean temperature shown in Fig. 6.2, where the contour lines of equal temperature are labeled in Fahrenheit. As apparent from Fig. 6.2, the mean annual temperature exhibit a marked spatial pattern, with the colder temperature in the mountains in the North-West

gently sloping toward Carolina coast line in the South-West. The temperature exhibits significant variations in both space and time, requiring that the mortality/temperature association be analyzed in the full spatiotemporal context of the vector random field model proposed in this work.

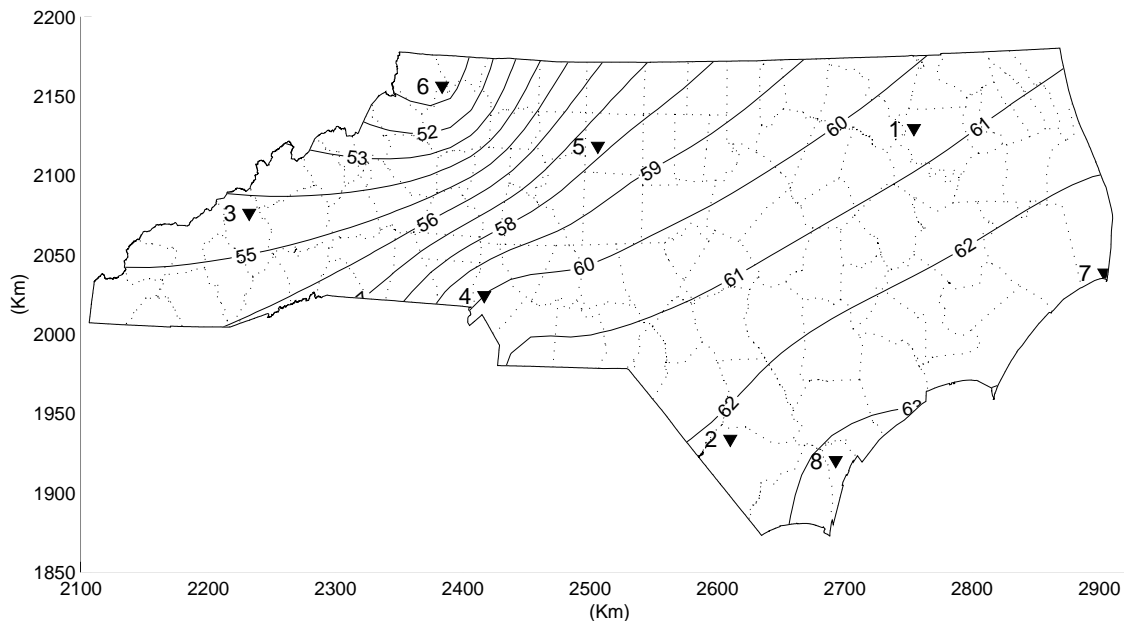


Figure 6.2: Map of yearly temperature average in North Carolina and weather stations. Contour lines of equal temperature are shown labeled in degree Fahrenheit, and triangles show the location of the weather stations, numbered 1 to 8.

Daily death of residents of North Carolina were extracted for the 1995-1996 calendar years from the mortality files provided by the North Carolina Center for Health Statistics. Death from accidental causes according to the *International Classification of Diseases*, Ninth Revision (ICD-9), codes >800 and out-of-state deaths were excluded from the analysis. The daily counts of death were recorded by county of residence for each of the 731 days of the 1995-1996 period. Counts of death on a daily basis are necessary in order to capture the temporal structure of the mortality/temperature association, however this results in many counts of zero daily death for the counties with small population. To overcome this problem, counties with small population were aggregated with the closest of

the 14 selected counties shown with filled circles in Fig. 6.1. These 14 counties were selected by choosing the 11 counties with the largest population (numbered 1 to 11 in Fig. 6.1), and adding the counties numbered 12 to 14 to provide an adequate coverage of the study area. This resulted in a set of selected counties with a balanced distribution of aggregated population (ranging from 69,288 residents aggregated to county 12, to 921,376 for county 2), and a small incidence of zero daily death counts (less than 0.6 % of days with zero death for the 14 counties over the 731 days period).

In order to study the spatiotemporal causal association between (colder) temperature and its health effect, we need to specify a measurable Space/Time Random Field (S/TRF) to model the health effect. The measurable S/TRF we use in this case study is referred to as the *death rate* $D(s,t)$, where s represents the spatial location, and t is the time. The death rate $D(s,t)$ is defined as the frequency at which people die at location s and time t , and has units of number of death per 100,000 people per day. However the information available are daily counts of death for the 14 selected counties and their aggregated neighbors. In order to obtain measured value of $D(s,t)$, we assume that the daily death count at a given county (divided by the number of residents --in 100,000s-- in that county) provides a reasonable measured value for the S/TRF $D(s,t)$ at the location of the centroid of that county --the filled circles in Fig. 6.1. The vector random field associated with the death rate is simply the Fahrenheit temperature $F(s,t)$ (temperature expressed in degree Fahrenheit), as measured directly at the eight weather stations shown in Fig. 6.2. To illustrate this association we plot in Fig. 6.3a the average death rate for North Carolina and in Fig. 6.3b the average Fahrenheit temperature for the 731 days period, where the average death rate is calculated as average of the measured death rate at each of the 14 locations shown with filled circles in Fig. 6.1, and the average Fahrenheit temperature is the arithmetic average of the recorded daily mean temperature at each of the eight weather stations shown in Fig. 6.2. The comparison of Fig. 6.3a and Fig. 6.3b suggest the

association between colder temperature (note the reverse y-axis scale used in Fig. 6.3b) and death rate. In the following we define the "scaled" temperature random field $T(s,t) = -K F(s,t)$, where $K = 4.4729 \times 10^{-2}$ is an arbitrary constant chosen such that the measured $K F(s,t)$ have the same average value as the measured death rates, and where the negative sign ensure a positive correlation between death rate $D(s,t)$ and scaled temperature $T(s,t)$, e.g. increased $T(s,t)$ are associated with increased $D(s,t)$.

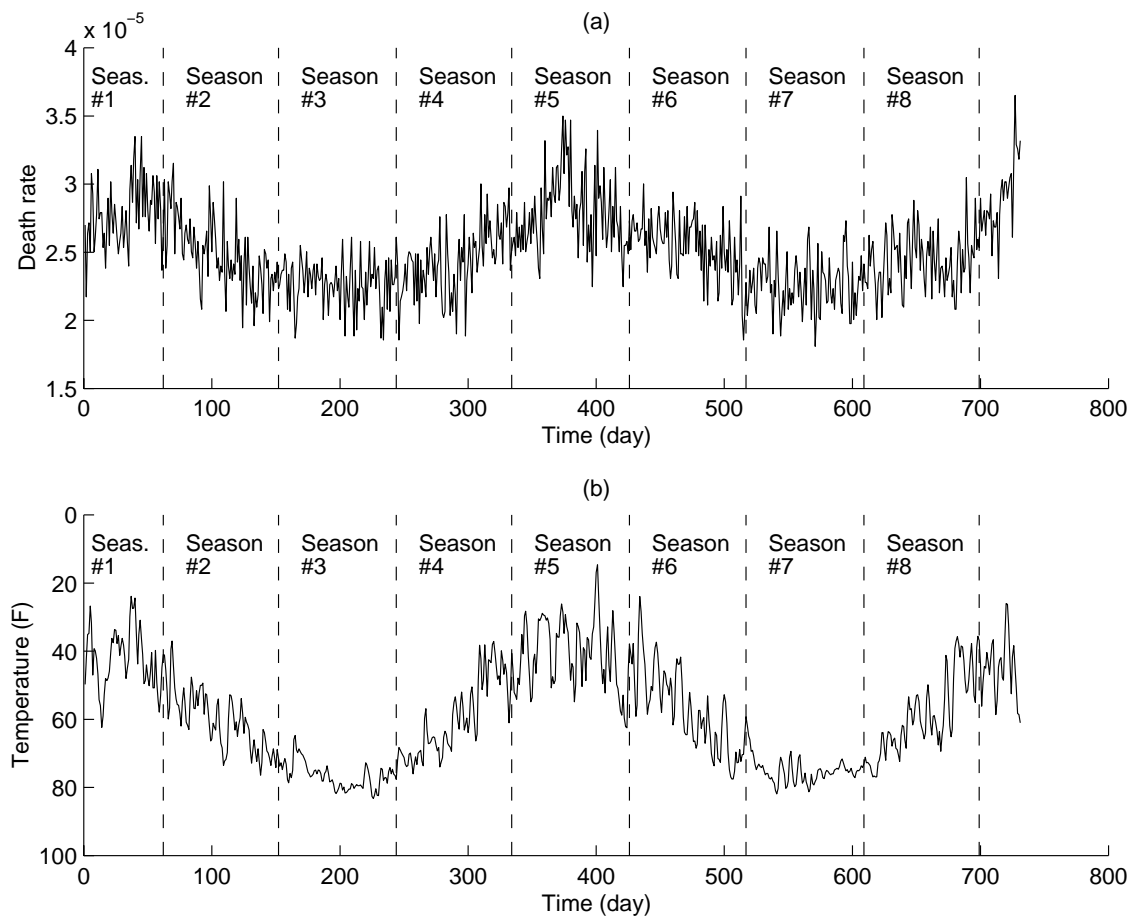


Figure 6.3: Time plots of average death rate and temperature for the state of North Carolina for the 1995-1996 time period. (a) Average of recorded death rates for the state expressed in # of death per people per day, (b) Average temperature over all weather stations.

The objective of this case study is to investigate the causal association between $T(s,t)$, referred to as the "temperature" in the following, and the death rate $D(s,t)$. In order to perform the vector random field analysis presented herein, we need to first specify

models for the covariance functions for the death rate and temperature, as well as their cross-covariance function. In order to facilitate the analysis, the 731 days time period covering the calendar year 1995-1996 is divided in 8 seasons as shown in Fig. 6.3. We note that season 1 and 5 (corresponding roughly to winter seasons), and seasons 3 and 7 (corresponding roughly to summer seasons) may be reasonably modeled using homogeneous covariance functions, e.g. of the form $C_X(s,t;s',t') = C_X(r, \tau)$, where $r = |s' - s|$ is the spatial lag and $\tau = t' - t$ is the time lag. The covariance function for $D(s,t)$ and $T(s,t)$ are estimated by

$$c_x(r, \tau) \approx \frac{1}{N(r, \tau)} \sum_{i=1}^{N(r, \tau)} (X_{-(r, \tau), i} X_{+(r, \tau), i}) - m_{-(r, \tau)} m_{+(r, \tau)}, \quad (6.20)$$

where x represents either the $D(s,t)$ or $T(s,t)$ field, $N(r, \tau)$ is the number of pairs of observed values $(X_{-(r, \tau), i}, X_{+(r, \tau), i})$ separated by the spatial and temporal lags r and t , $m_{-(r, \tau)}$ is the mean of the $X_{-(r, \tau), i}$ values and $m_{+(r, \tau)}$ is the mean of the $X_{+(r, \tau), i}$ values.

The covariance for death rate, $C_D(r, \tau)$, calculated for season 5, is shown in Fig 6.4, where the circles represents experimental values calculated via Eq. (6.20), and the plain line represents a theoretical covariance function fitting the experimental values. This covariance function is written as the following separable exponential function

$$C_D(r, \tau) = C_1 \delta_{r=0} \delta_{\tau=0} + C_0 \exp(-r / a_r) \exp(-|\tau| / a_t) \quad (6.21)$$

where $C_1 = 0.56$, $C_0 = 0.04$, $a_r = 200$ Km and $a_t = 6$ for season 5; and $C_1 = 0.59$ and $C_0 = 0.01$ for season 7.

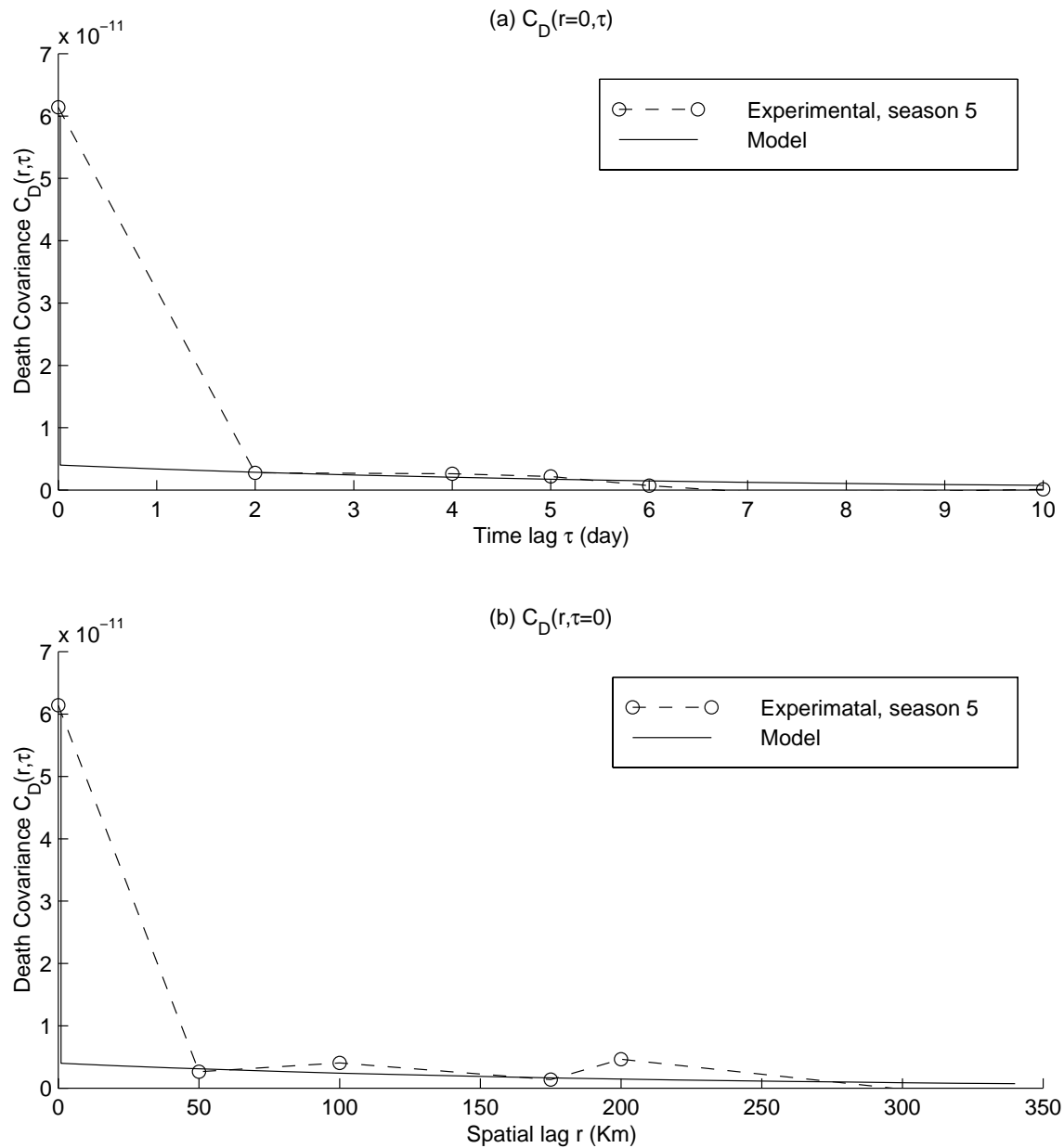


Figure 6.4: Space/time covariance for the death rate $D(s, t)$ random field for season 5, experimental values are shown with circles and theoretical model in plain line. (a) Covariance as a function of time lag for a zero spatial lag, (b) Covariance as a function of spatial lag for a zero time lag.

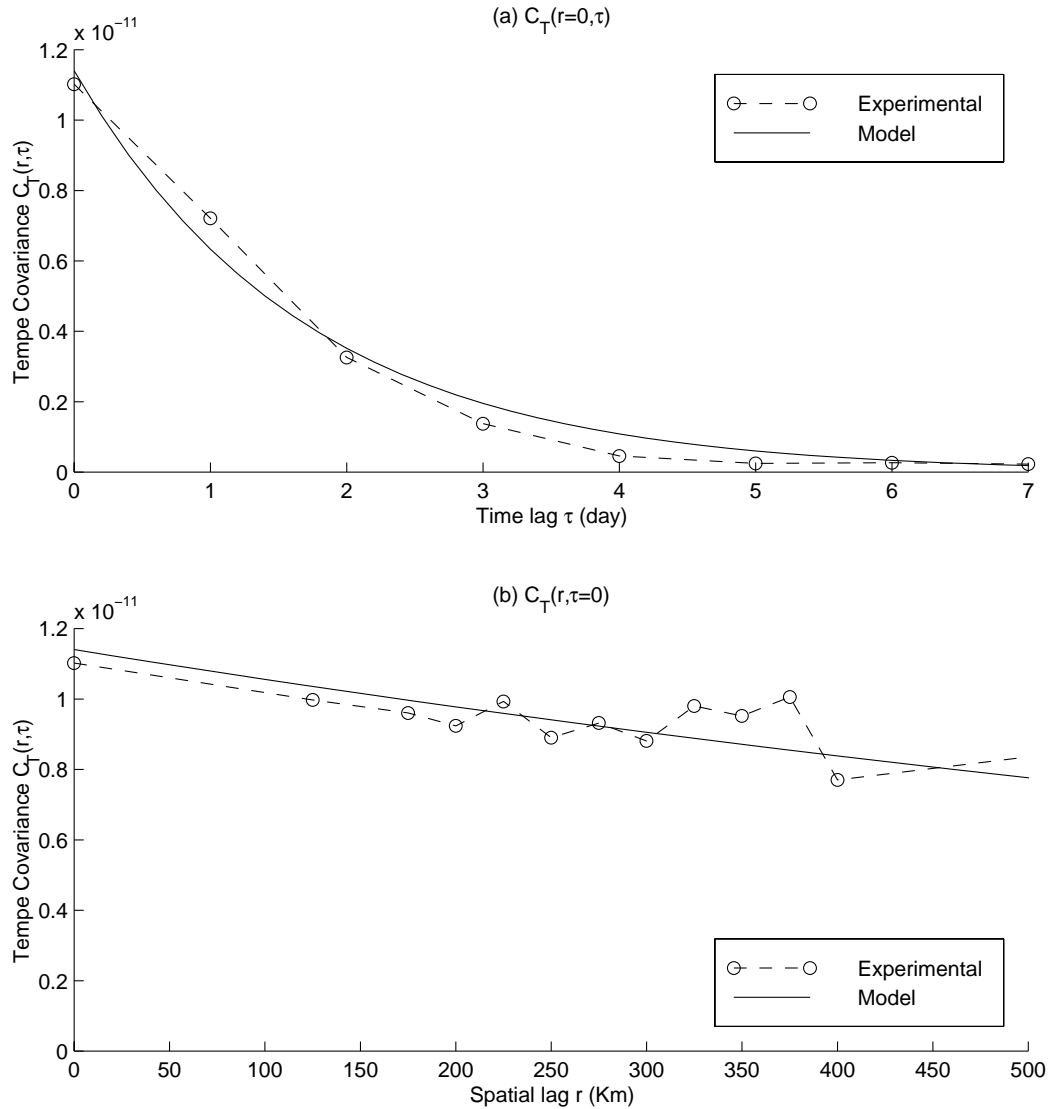


Figure 6.5: Space/time covariance for the scaled temperature $T(s,t)$ random field for the 1995-1996 time period, experimental values are shown with circles and theoretical model in plain line. (a) Covariance as a function of time lag for a zero spatial lag, (b) Covariance as a function of spatial lag for a zero time lag.

The covariance for the (scaled) temperature, $C_T(r, \tau)$, calculated for the entire 731 days period, is shown in Fig. 6.5. The theoretical covariance model chosen in this case is given as

$$C_T(r, \tau) = C_0 \exp(-r/a_r) \exp(-|\tau|/a_t) \quad (6.22)$$

with $C_0 = 0.11$, $a_r = 1300$ Km and $a_t = 1.7$ days, valid for all seasons. Finally we need to calculate the temperature/death-rate cross-covariance $C_{TD}(r, \tau)$. Experimental values are calculated using Eq. (6.20) by replacing x with TD, and taking care to include only temperature data in the "head" values $X_{-(r,\tau),i}$, and death rate data only for the "tail" values $X_{+(r,\tau),i}$. Experimental values calculated for season 5 and 7 are shown in Fig. 6.6 with circles and triangles, respectively. The theoretical covariance function fitting the experimental data is represented with a plain line, and corresponds to the following gaussian separable function

$$C_{TD}(r, \tau) = C_0 \exp(-r^2 / a_r^2) \exp(-(\tau - \tau_0)^2 / a_t^2) \quad (6.23)$$

with $C_0 = 0.036$, $a_r = 200$ Km, $a_t = 4$ days and $\tau_0 = 2$ days for season 5, and $C_0 = 0.009$ and $\tau_0 = 4$ day for season 7. The covariance functions (Eq. 6.21-6.23) are physically meaningful and a few comments are warranted. The $D(s,t)$ is characterized with a large nugget effect (e.g. C_1 much greater than C_0) while the $T(s,t)$ has no nugget effect, which indicate that $D(s,t)$ exhibits a large randomness while $T(s,t)$ is a smoother random field. The cross-covariance function $C_{TD}(r, \tau)$ reaches its maximum value for a time lag between temperature and death rate of τ_0 , with $\tau_0 = 2$ days in the winter and $\tau_0 = 4$ days for the summer. This mean that there is a time delay between a cold temperature episode and the resulting increase in death rate, indicative of the causal association under scrutiny.

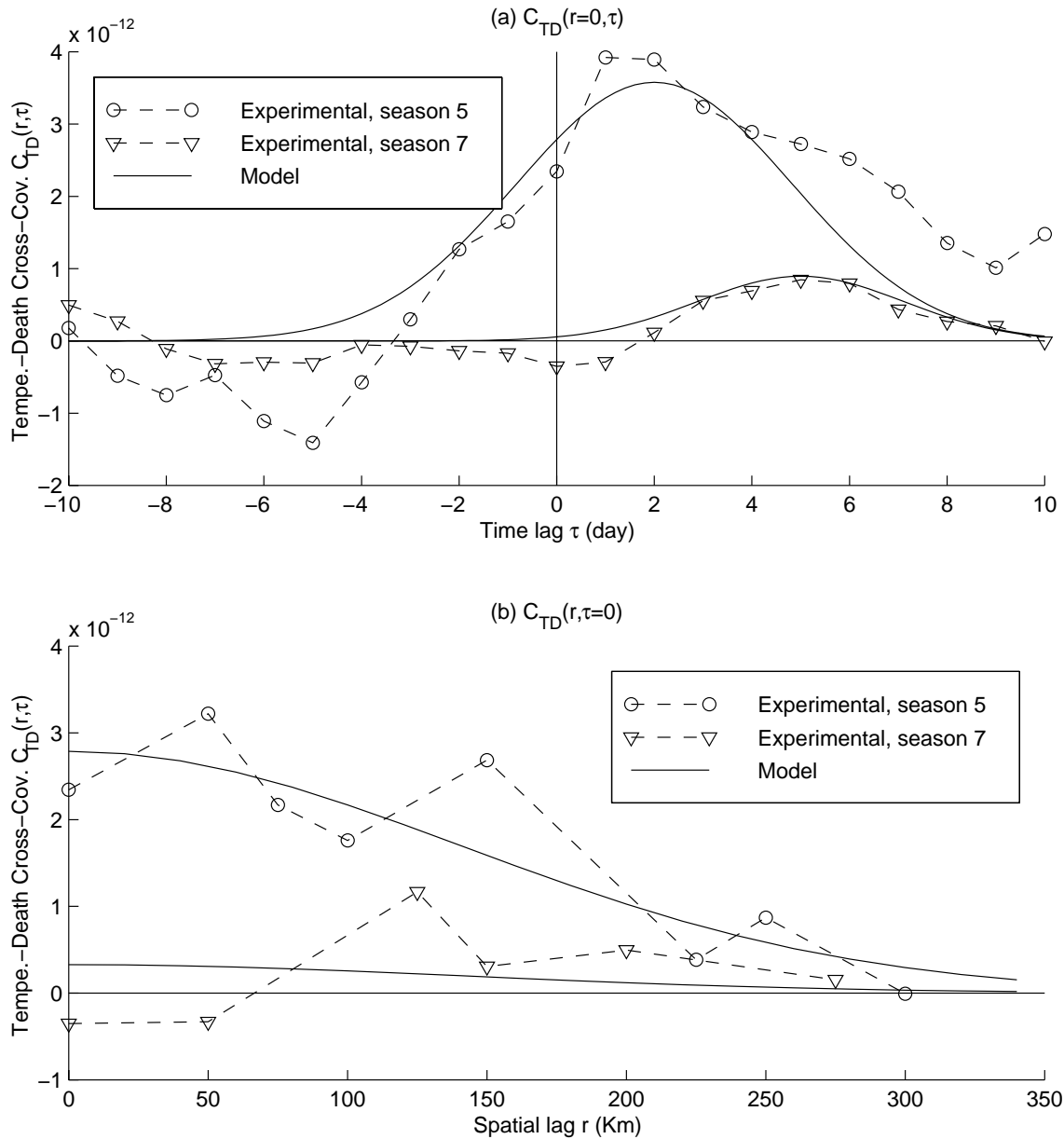


Figure 6.6: Space/time cross-covariance for the scaled temperature $T(s,t)$ and the death rate $D(s,t)$ for seasons 5 (circles), and season 7 (triangles), theoretical model in plain line. (a) Covariance as a function of time lag for a zero spatial lag, (b) Covariance as a function of spatial lag for a zero time lag.

According to the framework for vector random field analysis presented herein, we need to calculate the estimate $\hat{D}_D(s,t)$ for the death rate using only death rate data, and the estimate $\hat{D}_{DT}(s,t)$ using both temperature and death rate data. However we note that the measured values for $D(s,t)$ are actually daily death counts d_i within a county i , divided by the number of residents in 100,000 people units n_i of that county - if, e.g, there are 200,000 residents, then the number of residents in 100,000 people units is $n_i = 2$. As mentioned earlier we assumed that d_i / n_i provides a reasonable measurement value for the actual random field $D(s_i,t)$ at the centroid location s_i of county i . However d_i / n_i is an uncertain measurement for $D(s_i,t)$, and a more accurate representation of the reality is given by

$$(d_i - 1) / n_i < D(s_i,t) < (d_i + 1) / n_i . \quad (6.24)$$

This type of uncertain measurements are referred to as soft data. Consider for example the soft data represented with error bars in Fig. 6.7a for county 2, and in Fig 6.7b for county 12. Since county 12 has a much smaller population than county 2, the measurements for death rate at the centroid of county 12 have a larger uncertainty than the death rate measurements obtained in county 2. Soft data shown in Fig. 6.7 is of the interval type, and it can be rigorously taken in account using the vector BME approach. Using the BME approach, one calculates the posterior probability distribution function (pdf) $f_D(D_k)$ for the death rate D_k at an estimation point $\mathbf{p}_k = (s_k, t_k)$ using soft (interval) measurements of the death rate $\mathbf{D}_s = [D_{s,1}, \dots, D_{s,n_D}]$ at points $\{\mathbf{p}_{s,1}, \dots, \mathbf{p}_{s,n_D}\}$. The posterior pdf is given by the equation

$$f_D(D_k) = A^{-1} \int_{D_{s,l}}^{D_{s,u}} d\mathbf{D}_s \phi(\mathbf{D}_s; \mathbf{B}_{s|k} D_k, \mathbf{C}_{s|k}) \quad (6.25)$$

where A is a normalization constant, $\phi(\cdot)$ is the multivariate Gaussian pdf, $\mathbf{B}_{s|k} = \mathbf{C}_{D_s D_k} \mathbf{C}_{D_k D_k}^{-1}$, $\mathbf{C}_{s|k} = \mathbf{C}_{D_s D_s} - \mathbf{B}_{s|k} \mathbf{C}_{D_k D_s}$, and \mathbf{C}_{XY} in general represents the covariance matrix between vectors \mathbf{X} and \mathbf{Y} , such that if e.g. $\mathbf{X} = [X_1]$ and $\mathbf{Y} = [Y_1; Y_2]$ then $\mathbf{C}_{XY} = \begin{bmatrix} C_{X_1 Y_1} & C_{X_1 Y_2} \end{bmatrix}$ (note that bold face is used to specify a vector or matrix). Consider for example the posterior pdf shown in dotted line in Fig. 6.8, calculated for county 7 at day 415. The posterior pdf represents our state of knowledge about the possible values of the death rate D_k at the estimation point, *given* the soft (interval) measurements for the death rate at neighboring counties as well as for the same county but different days. From the posterior pdf $f_D(D_k)$ we obtain a BME mode estimate $\hat{D}_D(s_k, t_k) = 2.77$ by selecting the mode of the posterior pdf.

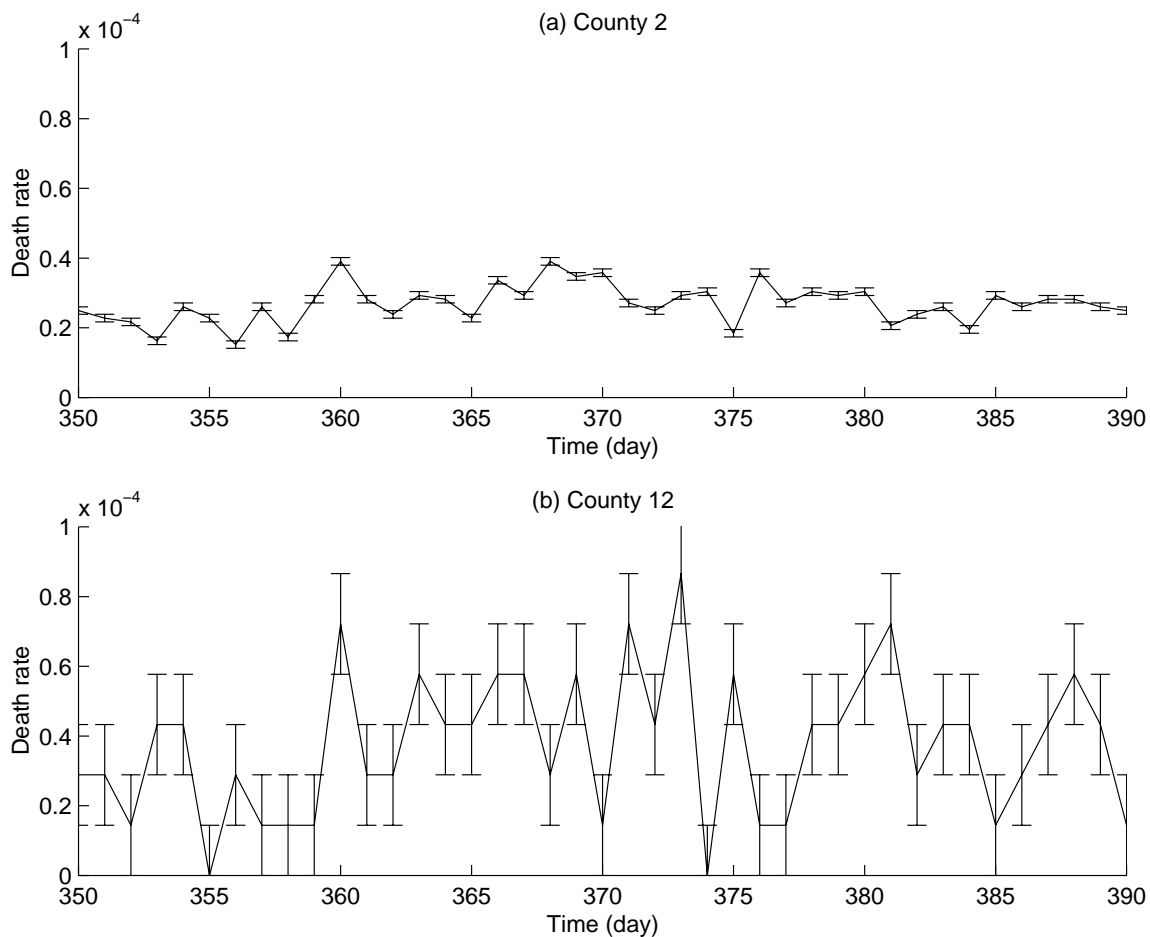


Figure 6.7: Death rate measurements for (a) county 2 and (b) county 12. Death rates are expressed in # death per people per day. The error bars represent the uncertainty in the measurements.

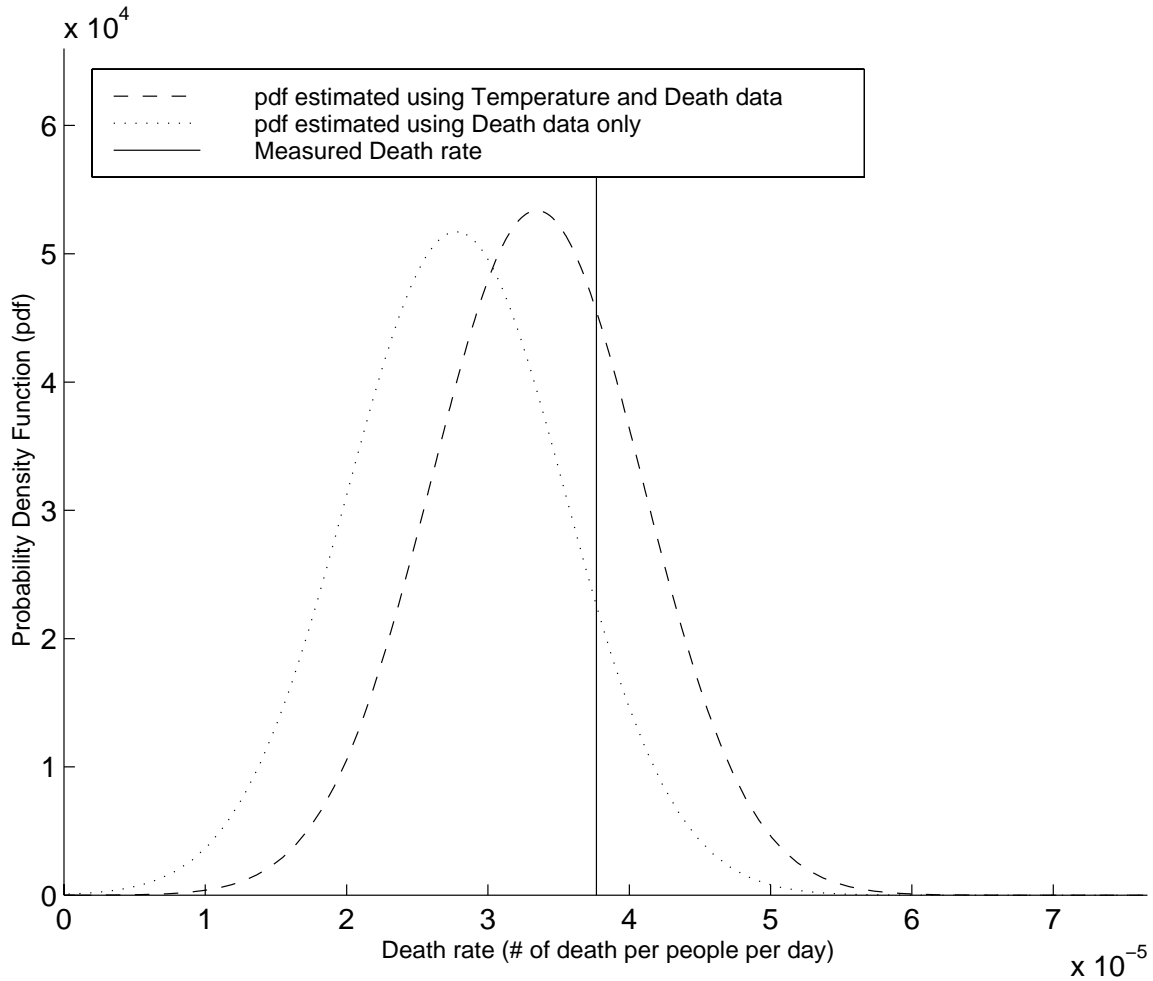


Figure 6.8: BME posterior pdf of the death rate for county 7, day 415. The vertical plain line represents the actual recorded death rate. The dotted line is the pdf calculated using only death rate data from neighboring counties and days. The dashed is obtained using both death rate and temperature data from neighboring counties and days.

Similarly we can use both death rate data and temperature data in the vector BME approach to calculate the posterior pdf $f_{DT}(D_k)$, using the soft data D_s and the temperature data $T_h = [T_{h,1}, \dots, T_{h,n_T}]$ at points $\{p_{h,1}, \dots, p_{h,n_T}\}$, where the subscript h signifies that these are *hard* (i.e. exact) measurements. The posterior pdf is in this case given by

$$f_{DT}(D_k) = A^{-1} \phi(D_k; \mathbf{B}_{k|h} \mathbf{T}_h, C_{k|h}) \int_{D_{s,l}}^{D_{s,u}} d\mathbf{D}_s \phi(\mathbf{D}_s; \mathbf{B}_{s|kh} [D_k; \mathbf{T}_h], C_{s|kh}) \quad (6.26)$$

where A is a normalization constant, $B_{k|h} = C_{D_k T_h} C_{T_h T_h}^{-1}$, $C_{k|h} = C_{D_k D_k} - B_{k|h} C_{T_h D_k}$, $B_{s|kh} = C_{D_s [D_k; T_h]} C_{[D_k; T_h] [D_k; T_h]}^{-1}$, and $C_{s|kh} = C_{D_s D_s} - B_{s|kh} C_{[D_k; T_h] D_s}$. As shown in Fig. 6.8, the pdf $f_{DT}(D_k)$ (represented with a dashed line) is an improvement over $f_D(D_k)$, and leads to a mode estimate $\hat{D}_{DT}(s_k, t_k) = 3.34$ that is closer to the measured death rate of 3.76 at county 7, day 415, depicted with the plain vertical line. In this example (county 7, day 415) the prediction error for the estimate $\hat{D}_{DT}(s_k, t_k)$ is smaller than that of $\hat{D}_D(s_k, t_k)$, which supports the causal association of colder temperature to death rate. However this is an isolated example, and in order to draw a conclusion, we need to compare the estimation errors in a way that is statistically significant. This is considered next.

Using the approach explained insofar, we calculate the estimated values $\hat{D}_D(s_k, t_k)$ and $\hat{D}_{DT}(s_k, t_k)$ at all 14 selected counties (Fig. 6.1) and all days of season 5 and season 7. At each estimation point (i.e. each county and each day), we estimate $\hat{D}_D(s_k, t_k)$ using soft death rate measurements from the neighboring counties and for the same county but different days. For $\hat{D}_{DT}(s_k, t_k)$ we include the same death rate data as well as temperature data available for the previous 2 to 5 days. Using the estimated values we calculate at each estimation point the estimation error by subtracting the death rate actually measured at the estimation point (which was ignored during the estimation), i.e. $e_D(s_k, t_k) = |\hat{D}_D(s_k, t_k) - d_k / n_k|$ and $e_{DT}(s_k, t_k) = |\hat{D}_{DT}(s_k, t_k) - d_k / n_k|$, where d_k is the daily count of deaths and n_k the number of resident living in the county corresponding to the estimation point s_k . The causal association between colder temperature and death rate is then investigated by computing the difference $E_{DT} - E_D$, where E_{DT} and E_D are the arithmetic average of the e_{DT} and e_D values over some space time domain. Negative values for $E_{DT} - E_D$ will support the mortality/temperature causal association whereas zero values would disprove the causal association.

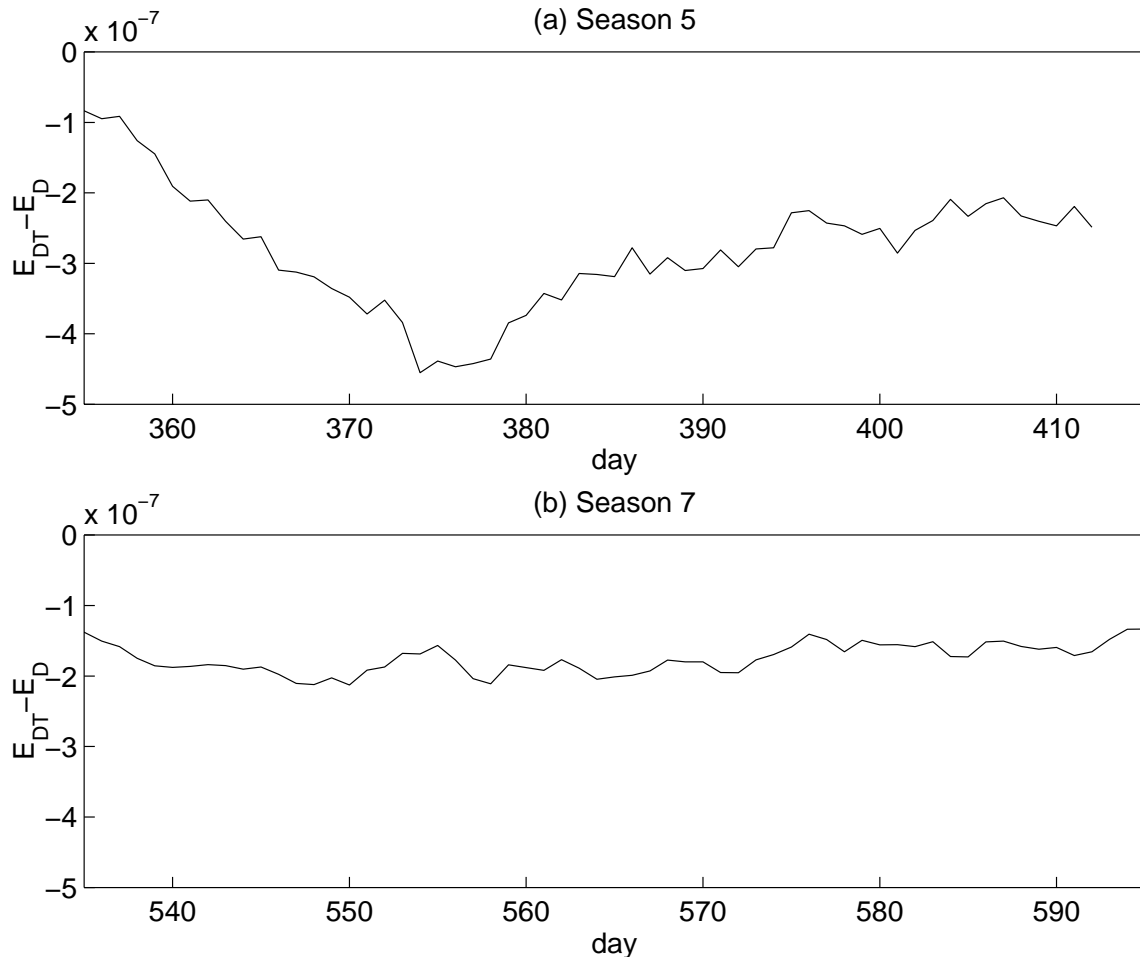


Figure 6.9: Time plots of $E_{DT} - E_D$, where E_{DT} is spatial average for North Carolina of estimation errors using both temperature and death rate, and E_D is when only death rate data is used, for (a) season 5, and (b) season 7.

In Fig. 6.9 we plot $E_{DT} - E_D$ as a function of time for season 5 (Fig. 6.9a) and season 7 (Fig. 6.9b). The space/time domain used to average the estimation error consist of all the spatial domain (i.e. all 14 counties) and a time window of 30 days, which results in $14 \times 30 = 420$ values to calculate the averages E_{DT} and E_D . Fig. 6.9 supports the mortality/temperature association for both seasons, since $E_{DT} - E_D$ is consistently negative (and therefore E_{DT} consistently smaller than E_D). Furthermore the magnitude of $E_{DT} - E_D$ is indicative of the strength in the mortality/temperature association, and it is noted that while the association is weaker and somewhat constant during summer (season 7), it is stronger and somewhat uneven during winter (season 5). In Fig. 6.10-6.11 we

investigate the mortality/temperature association in the spatial domain, by showing maps with contour lines of equal $E_{DT} - E_D$ values. In this case the averages E_{DT} and E_D are calculated for each of the 14 counties using all the e_{DT} and e_D values available for the relevant season, which consists of 93 values for season 5 and for season 7. Again the map of $E_{DT} - E_D$ for winter (season 5, Fig 6.10) portrays a stronger mortality/temperature association than that of the summer season (season 7, Fig. 6.11). However we also note that the association is weaker during the winter season on the eastern side of the state along the coast-line, probably due to the moderating effect of the ocean on cold temperature, while it is stronger on the Western side along the mountain ranges of the Great Smoky Mountains National Park.

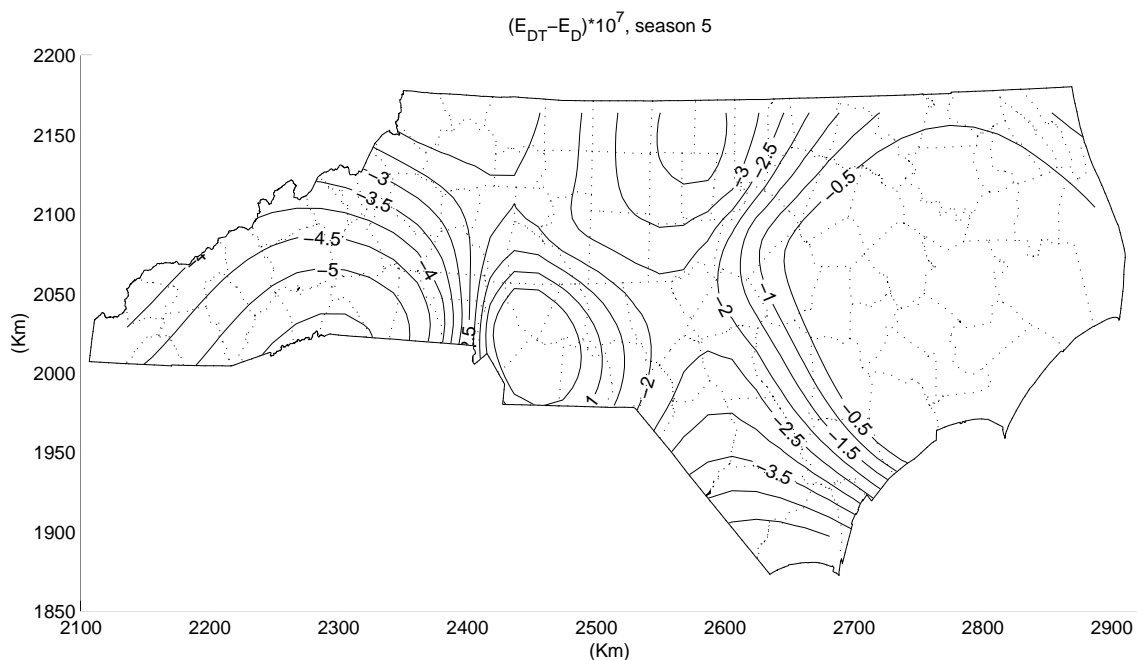


Figure 6.10: Map of $E_{DT} - E_D$, where E_{DT} is time average for season 5 of estimation errors using both temperature and death rate, and E_D is when only death rate data is used. Contour lines of equal values for $E_{DT} - E_D$ are labeled using units of # of death per people per day.

